We are IntechOpen,
the world's leading publisher of
Open Access books
Built by scientists, for scientists

4,800
Open access books available

122,000
International authors and editors

135M
Downloads

Our authors are among the

154
Countries delivered to

TOP 1%
most cited scientists

12.2%
Contributors from top 500 universities

CLARIVATE ANALYTICS
BOOK CITATION INDEX
INDEXED

WEB OF SCIENCE™

Selection of our books indexed in the Book Citation Index
in Web of Science™ Core Collection (BKCI)

Interested in publishing with us?
Contact book.department@intechopen.com

Numbers displayed above are based on latest data collected.
For more information visit www.intechopen.com

IFOG and IORG Gyros: A Study of Comparative Performance

Ramón José Pérez Menéndez

Abstract

In this revision work, firstly classical structure and main performance parameters of interferometric fiber-optic gyroscope (IFOG) and integrated optics passive resonator gyroscope (IORG) are reviewed. Then, the main advanced models and performance parameters of these two types of rotation-rate inertial sensors are described, and finally the design trends of both types are analyzed. Taking as reference the performance parameters analyzed above, a comparative analysis between manufactured IFOG and IORG units of close geometrical dimensions is realized. This analysis leads ranking these devices into six classical levels of inertial performance: strategic grade, navigation grade, high-end tactical grade, tactical grade, industrial low-end tactical grade, and consumer grade. This classification allows to deduce the main application areas of both kinds of devices. This way, the impact of these sensors in applications such as aeronautics, aerospace navigation, mechanical micro-fabrication, tactical weapons, or, more recently, robotics can be disclosed.

Keywords: interferometric fiber-optic gyroscope (IFOG), integrated optics passive resonator gyroscope (IORG), optical passive ring resonator interferometer, single-mode fiber (SMF), silicon wire waveguide

1. Introduction

Applications as guidance, navigation, and control systems in aircrafts, spacecrafts, and attitude systems in terrestrial vehicles, to give some examples, require compact, low cost, and reliable inertial navigation systems (INSs), which are equipped with increasingly accurate gyroscopes. For this reason, gyroscopes (in what follows from here, gyros) are key elements, which are essential to obtain the desired sensitivity for all above applications. Gyros having a dynamic range up to ±1500°/s are required in both space and terrestrial vehicle navigation inertial measurement units (IMUs). Attitude and heading systems in aircraft and precision-spacecraft INSs require a gyro resolution typically on the order of 1°/h and 0.01–0.001°/h, respectively. Optical gyros based on Sagnac effect are the key components of IMUs which are widely used in the above mentioned applications [1, 2]. Currently, the most widely used gyro technology for high-performance gyro systems is the optical fiber-based technology, specifically the technology based on interferometric fiber-optic gyro (IFOG). However, the counterpart of the IFOG made entirely in silicon wire waveguides on silicon-on-insulator (SOI) platform, called photonic integrated circuits (PICs) and, specifically, the integrated optics passive

resonator gyro (IORG), has many advantages such as high robustness, theoretical sensitivity, and superior reliability due to its inherent characteristics of miniaturized structure, all-solid-state, and the combination between integrated optics and well-known CMOS fabrication technology [3, 4]. Thus, IORG has been considered as the next generation of resonant micro-optical gyros (RMOG) and a promising candidate in the field of inertial navigation [3, 5]. In particular, IORGs are very promising in terms of performance parameters such as low cost, compactness, light weight, and high reliability.

Both of them (IFOGs and IORGs) are based on Sagnac effect, which generates a phase or frequency difference proportional to the angular rate when two counter-propagating light beams in an optical resonant cavity suffer a rotation. Sagnac effect has also been demonstrated in semiconductor ring laser gyros (SRLGs) [1, 6]. Passive optical resonators with the laser source external to the ring resonator are particularly attractive because they show high performance and overcome some issues of active devices, mainly lock-in effect and mode competition. So far, best demonstrated resolution for the IFOG is 0.0002°/h [IXSea, FOG Marins] for a strategic-grade unit with 5 km length and 200 mm fiber coil diameter [7], while for the IORG, the best value achieved is 1°/h [IntelliSense Corp., VIGOR] for a temperature-compensated high-end tactical-grade unit with weight < 100 g and volume < 5 cc. made on a silicon wire waveguide ring resonator [8].

This work is structured as follows: Sections 2 and 3 deal with the main structure and configurations of IFOG and IORG, respectively. Section 4 examines the performance-grade classification and parameters of IFOG and IORG. Section 5 collects the main performance parameters of IFOG and IORG units made or designed by the most important world manufacturers and laboratories, respectively, enabling a comparative study between them. Section 6 presents the main design advances, trends, and optimization issues in the IFOG and IORG cutting-edge engineering. Finally, Section 7 is devoted to extract the main conclusions of this work.

2. IFOG: basic structure and configurations

The interferometric fiber-optic gyro is to date a mature technology and was originally designed as a low-cost alternative to the ring laser gyro (RLG). Surprisingly, today IFOG can substitute the RLG both in terms of manufacturing costs and that of performance, gaining prominence in a series of military and commercial applications [9–12]. The studies provide that the developments in solid-state optics and fiber-optic technology could lead up to 0.0001°/h ultimate value in resolution performance for IFOG units even for small-size designs. The IFOG is based on the Sagnac effect within an open optical path realized by a N-turn fiber-optic coil when two independent counter-propagating light modes are externally introduced from a broadband laser source through its two ends, respectively (see **Figure 1**). This causes an interference pattern between the CW and CCW light beams to be collected in a photodetector with a phase shift given by the following equation:

$$\phi_S = \frac{2\pi L D}{\lambda_0\, c_0}\, \Omega \tag{1}$$

where L and D are length and diameter of fiber-optic sensing coil, respectively; λ_0 and c_0 are wavelength and speed of light source in vacuum, respectively; and Ω is the rotation rate.

For a fixed length L by fixing the coil diameter D, the sensitivity of the sensor can be improved by increasing the total coil length L by adding a high number of turns N taking into account an upper limit due to the fiber attenuation. Also working at 1310 nm wavelength instead of 1550 nm could help to improve the sensitivity of the sensor. From **Figure 1** it can be clearly seen that IFOG has a passive configuration because the laser source is located externally to the sensing coil. In this system, the two counter-propagating light beams travel through the core of a single-mode optical fiber (SMF) under the total internal reflection phenomenon. As the core diameter of such an optical fiber is only about 8 μm, the spot size of the interference signal can only be coupled to a small area at the end of the fiber loop, for example, on the small detection area of a photodetector. So that, this interference signal affects only one or two interference fringes whose intensity can be evaluated by the following expression:

$$I(\phi) = I_0(1 + \cos \phi) \tag{2}$$

where I_0 is the amplitude of each of the two counter-propagating beams and ϕ is the optical phase difference between them. **Figure 2** represents the variation of light
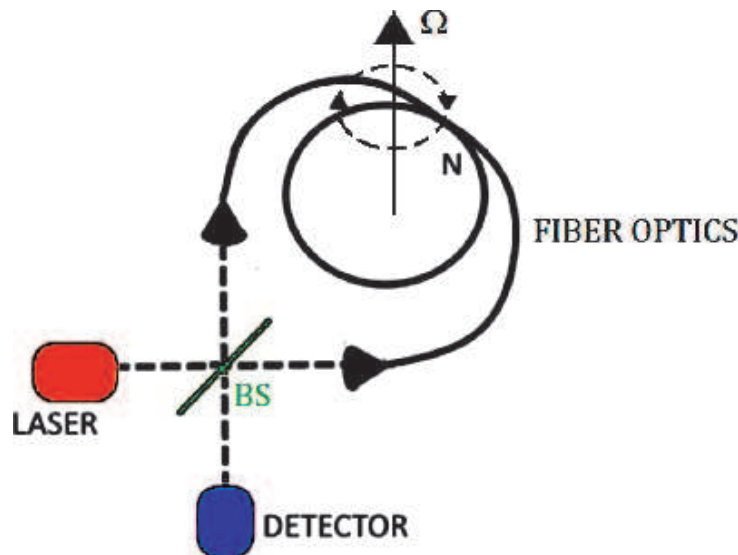

Figure 1.
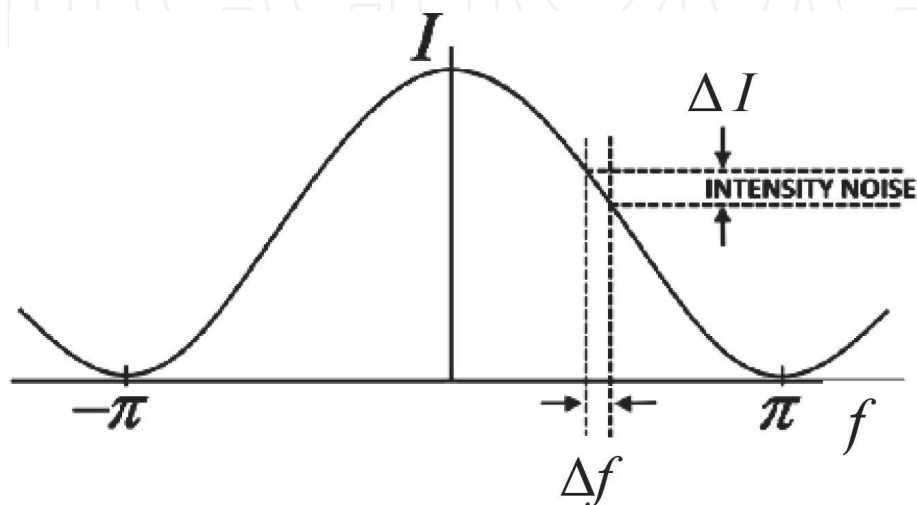*Basic structure of the IFOG.*

Figure 2.
Two-beam interference response curve as a function of ϕ (phase difference).

intensity along a single interference fringe as a function of ϕ. Notice the output intensity noise produced when the phase difference is detected with a phase error $\Delta\phi$. Phase noise sources and their influence are treated in Ref. [13].

Figure 3 shows the minimal open-loop IFOG unit configuration. This configuration includes apart fiber sensing coil, a superluminescent (SLD) broadband light source, two (2 input × 2 output) directional couplers, one linear polarizer, one photodetector, and one electro-optic phase modulator made of piezo ceramic tube (PZT) or lithium-niobate electrodes. The function of electro-optical phase modulator is to provide a controlled phase shift which adds to the Sagnac phase shift produced by the rotation onto the system.

This way, the signal detected by photodetector can be demodulated with some ease to recover by electronic means the Ω rotation-rate value which affects the whole system. A reduced minimal configuration fiber-optic gyro for land navigation applications can be found in Ref. [14]. Then two main options can be adopted for IFOG: open-loop configuration and closed-loop configuration. **Figure 4** represents one typical bulk optics open-loop IFOG configuration, the dotted block being usually made on an integrated optical chip (IOC). In this configuration, the rotation-rate information is recovered by the electrical output signal of photodetector after a previous demodulation process.

This configuration guarantees the reciprocity of the system. This implies that the two counter-propagating beams have exactly equal amplitude and phase at output when no rotation affects the system. However an error phase shift can be present on interferometric signal collected by the photodetector. So to reduce phase difference error and increase the resolution of the sensor, it is necessary to reach the
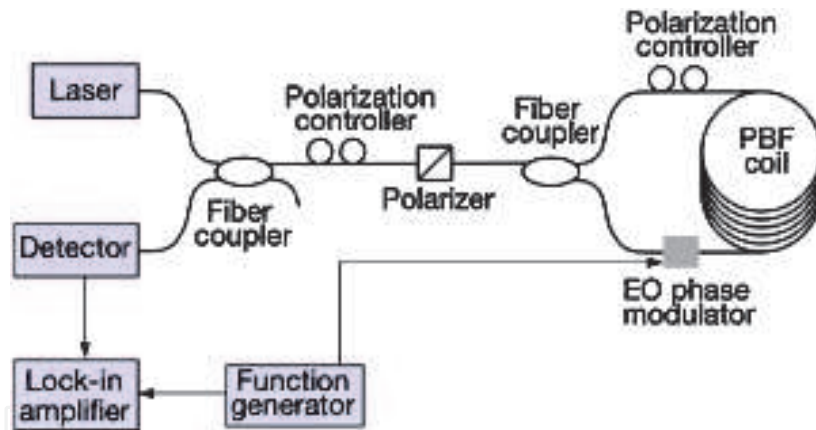

Figure 3.
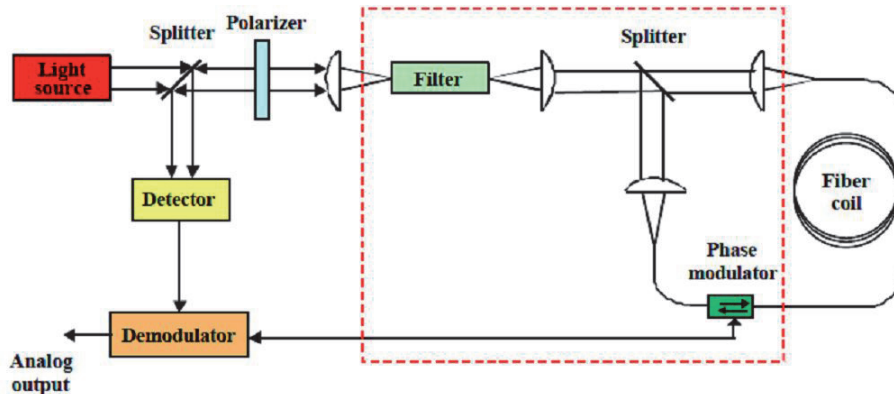*Minimal open-loop IFOG unit configuration.*

Figure 4.
Typical bulk optics IFOG open-loop configuration.

reciprocity condition as exactly as possible. Optical light source used is a broadband laser source to reduce the noise signal due to Rayleigh scattering within the fiber. As fiber sensing coil, either standard or rare-earth doped optical fiber can be used, but polarization-maintaining fiber is needed in both cases to ensure that just one polarization mode exists within it. The optical round trip experienced by the two counter-propagating beams is as follows. The light beam from source is collimated and coupled into an optical straight path and, then, passes through an optical system composed of one beam splitter, one linear polarizer, and a filter between two convergent lenses to select only one propagated mode within the fiber coil. The second beam splitter is used to split the original beam from the source and create two counter-propagated CW and CCW beams into the fiber coil. Then, after having traveled through the fiber loop, the CW and CCW beams recombine into the interferometer after passing again through the polarizer and reflecting onto the second face of splitter. Then, the photodetector collects the produced interferometric signal. The phase modulator is used to apply a sinusoidal or square-wave dynamic phase bias to light path, thus increasing the sensitivity of the sensor [15]. When modulation frequency of phase bias is high enough, electronic noise is avoided. Finally, an electronic demodulation circuit is needed to extract the magnitude and sign of rotation rate. Main advantages for the open-loop IFOG scheme are a few number of optical and electronic components and, hence, low price, good sensitivity, long lifetime, high reliability, and low power consumption. The main disadvantages of this configuration are high fiber coil length (100–3000 m) to increase sensitivity, electronic drift of analogical components, and disturbing influence of temperature and environmental conditions.

A more advanced design is achieved by closing the measurement loop by means of a feedback signal becoming into the so-called IFOG closed-loop configuration. The general scheme of a closed-loop IFOG is depicted in **Figure 5**. Very high performance was obtained for closed-loop IFOG configuration with respect the open-loop one [16]. In this scheme, the output signal of demodulator circuit passes through a servo amplifier which drives a phase transducer placed in the interferometer path. The total phase shift becomes equal to zero because the phase transducer introduces a nonreciprocal phase shift that is equal, by in the opposite sign, to that generated by Sagnac phase shift induced by rotation. The output of the system is then the output of the phase transducer. The main advantage of this configuration is the insensitivity to the laser source amplitude variations and the electronic circuitry gain because the system is always operated at zero total phase shift. This
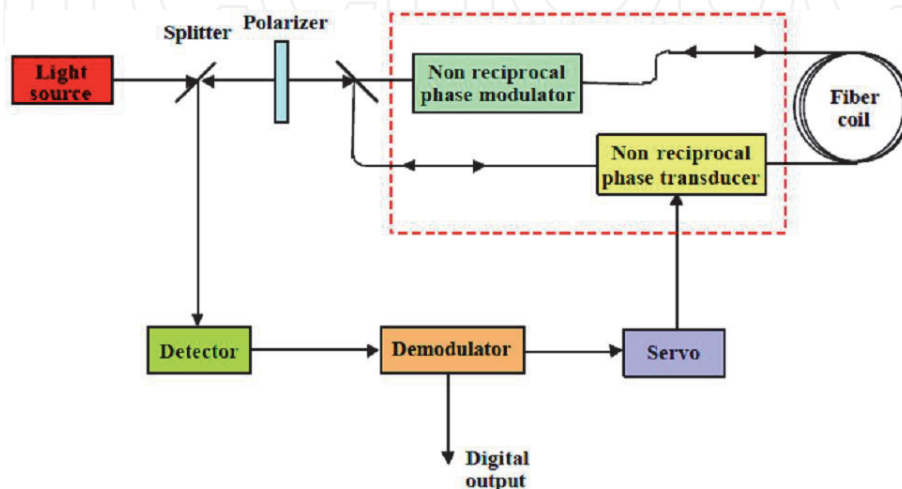

Figure 5.
Typical closed-loop IFOG configuration.

brings very small drift, from 0.001°/h up to 0.01°/h On the other hand, the output scale factor linearity and stability depends only on the phase transducer accuracy.

Eq. (3) allows the calculation of photon-shot-noise photocurrent at photodetector (I_{sn}), which is the minimum photodetector output current corresponding to a given level of optical input power:

$$I_{sn} = \sqrt{\frac{e^2 \eta \lambda}{h c} P_{\max} \Delta f} \qquad (3)$$

Here, $P_{\max}$ is the maximum optical power incident at photodetector, Δf is the minimum bandwidth detectable by the photodetector, and e, η, λ, h, and c are the electron charge, the quantum efficiency of photodetector, the operating vacuum wavelength, the Planck constant, and the vacuum speed of light, respectively. This way, in accordance with photon-shot-noise photodetector current, the $\delta\Omega$ threshold sensitivity of gyro sensor (that is to say, the minimum rotation rate which this gyro is able to measure) can be calculated by Eq. (4):

$$\delta\Omega = \left(\frac{h c^2}{\pi e \eta L D P_{\max}}\right) I_{sn} \qquad (4)$$

where L and D are the length and diameter of sensing fiber coil, respectively, and the other parameters are the same as in Eq. (3). From this expression it can be clearly seen that the greater the product L × D, the better the sensitivity of the detector. Thus, typical performance reported for open-loop and closed-loop IFOG configurations are ±100°/hr [17–21]. dynamic range, bias drift between 0.001°/h and 0.2°/h with drift stability between 0.0005°/h and 0.01°/h, angle random walk (ARW) between 0.004°/$\sqrt{\text{hr}}$ and 0.04°/$\sqrt{\text{hr}}$, and bandwidth from 20 to 100 Hz. Those IFOGs have long been used for land navigation applications mainly due to their extreme robustness, and also they are also commercially available for use in space applications due to their high reliability and cost-effectiveness.

3. IORG: fundamentals and main configurations

The usage of RFOGs instead of IFOGs is the first step that allows to reduce the fiber-optic coil length, thus leading to lower dimensions. Then, in the era of miniaturization, the possibility of integrating optical waveguides different than optical fibers leads to even smaller geometrical dimensions. Thus, RMOG is a promising candidate for applications requiring small, light, and robust gyros. The first design of an RFOG was made by S. Ezekiel and S.R. Balsamo at M.I.T. in 1977. In this design, the difference Δf between CW and CCW frequency resonances of the cavity is given by the following equation [22, 23]:

$$\Delta f = \left(\frac{4A}{\lambda P}\right) \Omega \qquad (5)$$

where A is the area enclosed by the cavity, P is the perimeter of the cavity, λ is the vacuum wavelength, and Ω is the rotation rate affecting the system. The precision with which Δf can be measured depends on the Q factor of the cavity. This way, the minimum rotation rate that this gyro is able to measure can be calculated by Eq. (6):

$$\delta\Omega \;=\; \frac{1}{Q\,D\sqrt{P_{pd}}}\sqrt{\frac{2hc^3}{\lambda\eta\tau}} \tag{6}$$

here Q is the Q factor of the cavity, D is its diameter, P_{pd} is the input optical power incident on photodetector, τ is the integration time, and h, c, λ, and η are the same as in Eq. (4). A new step to achieve the miniaturization of the gyro is to perform the passive ring resonator by means of an integrated optical waveguide made of high-index-contrast materials like silica-on-silicon, silicon-on-insulator, III–V semiconductors (InP), or silicon nitride (Si_3N_4). Then, this solution gets to what is called the IORG. Thus, an IORG can be formed by a ring resonator that includes an optical waveguide having a ring shape and one or two straight bus waveguides (see **Figure 6**). The bus and the ring waveguides are coupled by the evanescent field. When the ring is used for rotation sensing, it is necessary to launch two input signals (CW, CCW) simultaneously in the bus waveguides to excite the ring resonator cavity for both the CW and CCW propagation directions for the Sagnac effect to be applied.

If a two-bus waveguide approach is used, the two input beams can be launched in two different bus waveguides or in the two opposite ends of the same bus waveguide. Consequently there are two possible configurations for the excitation of the cavity and resonance frequency measurement. In the first case, output ports are called through ports (**Figure 6(a)** and **(c)**), whereas in the second one, output ports are the drop ports (**Figure 6(b)**). Using a one-bus waveguide architecture, each end of the bus can be utilized either as input or output port. In this case, two circulators or switches have to be used at both ends of the bus to excite the resonator in CW and CCW directions and to monitor the spectral response at the respective through port (**Figure 6(c)**). To minimize the bias drift of the gyro, the two beams coupled to the resonator must have the same optical power amplitude or as similar as possible with very reduced tolerance.

The conventional configuration of an IORG includes a narrow linewidth laser source, a high Q factor ring resonator, an optoelectronic processing unit, two photodetectors, and an electronic readout unit (**Figure 7**). The sensor can be manufactured by using hybrid or monolithic photonic integration. Hybrid integration has as main problems the optical alignment of all components and the high value of optical power losses. Monolithic integration has the advantages of the absence of optical alignment issues, the higher robustness and compactness, the minor dimensionality, and the lower optical power consumption.
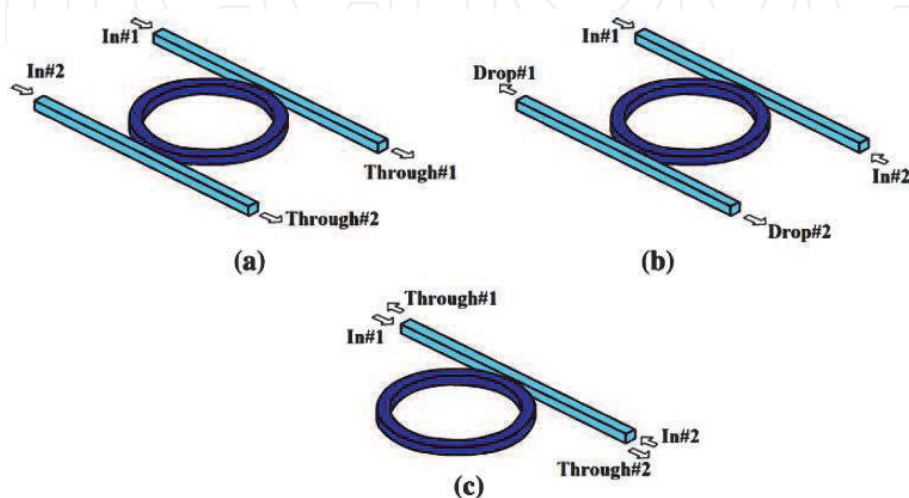

Figure 6.
Integrated ring resonator coupled with one (c) or two (a), (b) waveguides (sensing element of IORG).
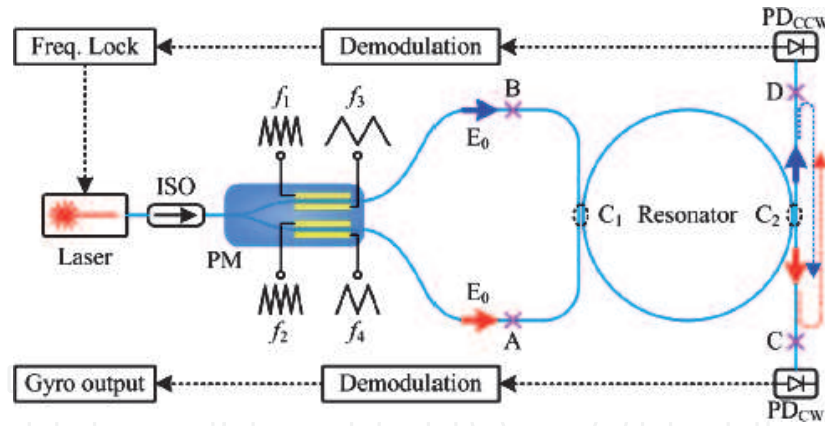
Figure 7.
Conventional configuration of an IORG, including a narrow linewidth laser source, an optical isolator, optoelectronic components for demodulation processing, a waveguide ring resonator, two detectors, and electronics readout unit.
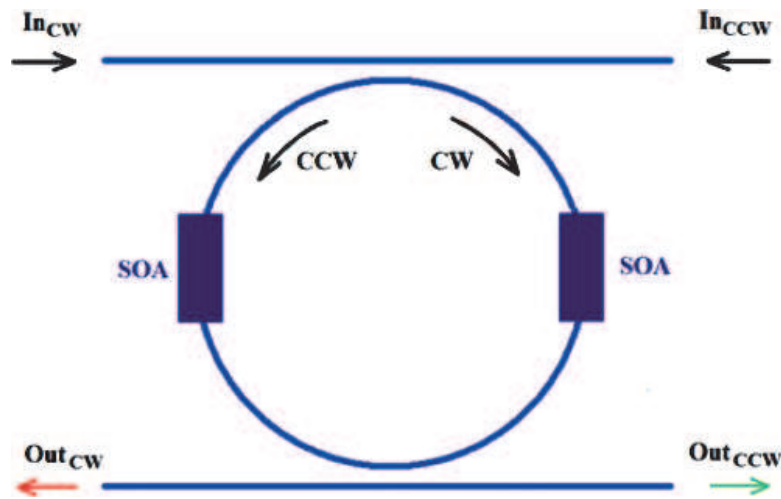

Figure 8.
Two SOAs are incorporated within ring resonator to compensate propagation loss.

The dimensions of the integrated passive resonator influence gyro scale factor, and, in time, the cavity Q factor depends on loss and resonator length. This way, to achieve $\delta\Omega < 5°/h$ and ARW $< 0.02°/\sqrt{h}$, a Q factor around 10^6 and a resonator length in the range of centimeters are at least required [24].

Maximum achieved Q factor in SOI ring resonators is around 1.5×10^5. This limitation in Q factor makes very difficult to realize a passive integrated optical gyroscope having $\delta\Omega < 5°/h$ by using a SOI ring resonator. On the other hand, silica-on-silicon technology allows very low loss (<0.1 dB/cm) operating at 1.55 μm, so that waveguides made on this technology are more suitable for IORG engineering. Propagation losses around 0.02–0.03 dB/cm have been achieved for low-index contrast silica-on-silicon waveguides ($\Delta < 1\%$). As bending loss suffered by these waveguides exponentially decreases with curvature radius, to achieve negligible bending loss, a curvature radius larger than a few millimeters is required. Some ring resonators employing a 5 μm × 5 μm squared core having a very large quality Q factor (2.4×10^7) and operating at 1.55 μm wavelength have been fabricated in silica-on-silicon technology. To further enhance the Q factor of resonators in silica-on-silicon technology, the hybrid integration of two semiconductor optical amplifiers (SOAs) within a silica-on-silicon ring resonator was proposed (**Figure 8**).

For a ring radius of 10 mm and a cross-coupling coefficient of 0.001 between, a Q factor as high as 2.9×10^8 was calculated, neglecting the effect of spontaneous

emission noise. Then, with this ring resonator configuration, an IORG unit exhibiting 10°/h bias drift was achieved. A spiral resonator having a total length of 42 cm and a footprint of 20 cm^2 was designed in 2012 by Ciminelli et al. with an estimated bias drift equal to 0.2°/h, which is the best value reached to date for this kind of IORG [25]. A new trend of design over InP waveguide technology is emerging to improve the scale of integration of IORG, to come to make a true gyro-on-a-chip (GoC). However, substantial improvements have to be found in this technology because the best value calculated so far reaches a resolution of 10°/h.

4. IFOG and IORG: performance grade and parameters

Table 1 collects the six levels of gyro performance-grade classification together with its characteristic rotation-rate resolution. As it can be seen, each performance level includes scales by two orders of magnitude. For each of them, the main areas of application are detailed on the right column.

What follows next is a concise description of each gyro performance parameter. Four main gyro performance parameters will be considered here, namely, bias stability, scale factor linearity, angle random walk, and dynamic range. For one more deep analysis and exhaustive information about the definition of gyro performance parameters, the reader should consult [26].

4.1 Bias stability

Bias instability is the measurement of bias offset at any constant temperature and ideal environment. It can be measured using the Allan variance technique. Bias instability introduces errors that may not be easy to calibrate. Its influence is greater on longer measurement periods, so that bias instability is one of the most critical parameters in the gyro selection process for applications that require excellent accuracy over long time. Therefore, two values of bias stability are usually considered: (1) the long-term bias drift for long integration time values, say 1 min or 1 h, and (2) the short-term bias drift, say 1 s.

4.2 Scale factor linearity

The linearity of the scale factor is the maximum separation with respect to the linear variation of the rotation rate expressed in ppm (parts-per-million) or % (parts-per-cent).

Performance grade/bias stability range		Applications
Consumer	30–1000°/h	Motion interface
Industrial and low-end tactical	1–30°/h	Ammunitions and rocket guidance
Tactical	0.1–30°/h	Platform stabilization
High-end tactical	0.1–1°/h	Missile navigation
Navigation	0.01–0.1°/h	Aeronautics navigation
Strategic	0.0001–0.01°/h	Submarine navigation

Table 1.
IFOG and IORG: performance-grade classification and respective applications.

4.3 Angle random walk (ARW)

In the output of a gyro, there is always a broadband white noise element. Angle random walk describes the error resulting from this noise element and can be evaluated using the Allan variance technique. Active elements of the gyro are the major contributors to random noise (laser diode and photodiode for optical gyroscopes and the vibrating beam and detection electronics for MEMS). Noise is one of the most important differences between optical and MEMS gyro performance, resulting in different precision and accuracy in measurements.

4.4 Dynamic range

Dynamic range is the maximum excursion of rotation rate that the gyro is able to measure with a maximum error specified by the rotation-rate drift (bias stability).

5. IFOG and IORG performance parameters: a comparative analysis

Next, in **Table 2**, the performance parameters of 33 IFOG, RFOG, RLG, or IORG gyros are collected for comparison purposes. Five gyro performance parameters are considered here: bias stability, scale factor linearity, ARW, dynamic range, and dimensions/weight/response time. For each type of gyro unit, either manufactured or designed, the manufacturer and the main areas of application are also specified. In the case of the units manufactured, the performance parameters were obtained from the technical manufacturer data sheets, while for the units designed and tested in the laboratory, the data have been obtained from the referenced scientific publication.

6. IFOG and IORG: advanced design, trends, and optimization

In recent years, several groups of researchers throughout the world are devoting great effort in the development of high-performance resonant micro-optical gyros (RMOG). All of these RMOG designs are based on a waveguide/ring resonator structure acting as the sensor element of rotation rate. The main variants of this design are focused either on ultrahigh Q silica-on-silicon ($Q = 1.5 \times 10^6$) or InP ($Q \geq 10^6$) ring resonators or on Si waveguide/photonic crystal (PhC) ring resonator ($Q = 7 \times 10^8$). More explicitly, the very promising research field of IORGs aiming at the development of optoelectronic ultracompact and high-performance gyros compliant with the requirements of aerospace and defense industry is recently focused onto five technological approaches that are being explored: (1) SRLGs, (2) RMOGs based on ultrahigh Q silica resonators, (3) InP gyro-on-a-chip, (4) the gyro configuration based on the ring cavity with a Bragg grating in the resonant path, and (5) the multi-ring-cavity gyro. For all of them, main efforts focus on design improvement, efficient modulation technique, and resolution enhancement. It is expected that a gyroscope on-a-chip prototype will be developed soon. If the characterization of that prototype will be successful, it is expected that the gyro-on-a-chip will have a very notably impact on the aerospace and defense navigation applications.

IFOG/IORG gyro technology	Performance grade/bias stability range	IFOG/IORG parameters					Manufacturer [model]/researcher ref. [X]	Applications
		Bias stability	Scale factor linearity	Dimensions/weight/response time	ARW	Dynamic range		
IFOG	High-end tactical	0.1–1°/h	≤1°/h	≤10,000 ppm	18.8mm × 19.1 mm × 24.6 mm (L × W × H)/25 g	≤0.05°/√h	±200°/s	Northrop Grumman LITEF [G-2000]	Missile and platform stabilization
IFOG	Navigation	0.01–0.1°/h	≤0.07°/h	≤100 ppm	L = 200 m, D = 88.9 mm/ 750 g/no data	≤0.056°/√h	±11.46°/s	Litton [LN-200]	Aeronautics navigation
IFOG	Navigation	0.01–0.1°/h	≤0.04°/h	≤100 ppm	210.8 × 119.9 × 79.8 (L × W × H)/1950 g	≤0.002°/√h	±300°/s	Northrop Grumman LITEF [LR-240]	Image and platform stabilization
IFOG	Strategic	0.0001–0.01°/h	≤0.0009°/h	≤10 ppm	L = 1000 m, D = 76 mm/750 g	≤0.0009°/√h	±250°/s	Litton guidance and control systems [7]	Space navigation
RLG	High-end tactical	0.1–1°/h	≤1°/h	≤1 ppm	Volume = 541 cm^3/900 g	≤0.125°/√h	±358°/s up to ±1620°/s	Honeywell [HG1700IMU]	Missile navigation
IFOG	Strategic	0.0001–0.01°/h	≤0.0003°/h	≤1 ppm	L = 4000 m, D = no data/no data	≤0.00010°/√h	No data	Honeywell [HPFOG]	Space navigation
IFOG	Strategic	0.0001–0.01°/h	≤0.0007°/h	≤15 ppm	L = 1500 m, D = 180 mm /no data	≤0.00022°/√h	±30°/s	IXSea [FOG180]	Aeronautics navigation
IFOG	Strategic	0.0001–0.01°/h	≤0.0005°/h	≤30 ppm	L = 2000 m, D = 330 mm/no data	≤0.00021°/√h	±15°/s	IXSpace [ASTRIX200]	Space navigation
IFOG	Strategic	0.0001–0.01°/h	≤0.0002°/h	≤15 ppm	L = 5000 m, D = 370 mm/no data	≤0.00017°/√h	±15°/s	IXSea [FOG MarinsM3]	Submarine navigation
IFOG	Tactical	0.1–30°/h	≤5°/h	≤1000 ppm	L = 75 m, D = 58.42 mm/≤3 ms	≤0.14°/√h	±204°/s	KVH [DSP1500digital]	Platform stabilization
IFOG	Tactical	0.1–30°/h	≤3°/h	<500 ppm	L = 125 m, D = 58.42 mm/no data	≤0.10°/√h	±100°/s	KVH [DSP3000analog]	Platform stabilization

IFOG/ IORG gyro technology	Performance grade/bias stability range		IFOG/IORG parameters					Manufacturer [model]/ researcher ref. [X]	Applications
			Bias stability	Scale factor linearity	Dimensions/weight/response time	ARW	Dynamic range		
IFOG	Tactical	0.1–30°/h	≤1°/h	<500 ppm	L = 300 m, D = 58.42 mm/no data	≤0.067°/√h	±375°/s	KVH [DSP3000 digital]	Platform stabilization
IFOG	Navigation	0.01–0.1°/h	≤0.05°/h	≤500 ppm	L = 500 m, D = 45.97 mm/≤ 1.3 ms	≤0.013°/√h	±490°/s	KVH [DSP1750]	Aeronautics navigation
IFOG	Navigation	0.01–0.1°/h	0.10°/h (RMS)	50 ppm	L = 200 m, D = 81.2 mm/220 g	≤0.015°/√h	±1000°/s	Emcore [EMP-1]	Aeronautics navigation
IFOG	Strategic	0.0001–0.01°/h	0.005°/h (RMS)	25 ppm	L = 200 m, D = 83.8 mm/230 g	≤0.002°/√h	±1000°/s	Emcore [EMP-1.2 k]	Aeronautics/aviation
IFOG	Strategic	0.0001–.01°/h	0.0060°/h	≤300 ppm	L = 200 m, D = 78 mm/200 g	≤ 0.015°/√h	± 550°/s	Optolink [SRS-200]/[28]	Submarine navigation
IFOG	Strategic	0.0001–0.01°/h	0.0011°/h	≤200 ppm	L = 500 m, D = 100 mm/350 g	≤0.003°/√h	±250°/s ±1000°/s	Optolink [SRS-501]/[28]	Submarine navigation
IFOG	Strategic	0.0001–0.01°/h	0.0006°/h	≤100 ppm	L = 1000 m, D = 150 mm/900 g	≤0.0005°/√h	±550°/s	Optolink [SRS-1001]/[28]	Submarine navigation
IFOG	Strategic	0.0001–0.01°/h	0.00024°/h	≤30 ppm	L = 2000 m, D = 250 mm/ 1700 g	≤0.00026°/√h	±30°/s	Optolink [SRS-2000]/[28]	Space navigation
IFOG	Strategic	0.0001–0.01°/h	0.00008°/h	≤10 ppm	L = 5000 m, D = 250 mm/ 2500 g	<0.000069°/√h	±12°/s ±550°/s	Optolink [SRS-5000]/[28]	Space navigation
IFOG	Tactical	0.1–30°/h	30°/h (RMS)	100 ppm	L = 75 m, D = 24 mm/30 g/ 20 ms	≤0.090°/√h	±300°/s	Fizoptika [VG091A]/[29]	Platform stabilization
IFOG	Tactical	0.1–30°/h	20°/h (RMS)	100 ppm	L = 100 m, D = 60 mm/45 g/ 10 ms	≤0.040°/√h	±300°/s	Fizoptika [VG949P]/[29]	Platform stabilization
IFOG	Tactical	0.1–30°/h	10°/h (RMS)	100 ppm	L = 125 m, D = 82 mm/120 g/< 20 ms	≤0.015°/√h	±250°/s	Fizoptika [VG095M]/ [29]	Platform stabilization

IFOG/ IORG gyro technology	Performance grade/bias stability range		IFOG/IORG parameters					Manufacturer [model]/ researcher ref. [X]	Applications
			Bias stability	Scale factor linearity	Dimensions/weight/response time	ARW	Dynamic range		
IFOG	High-end tactical	0.1–30°/h	1.00°/h (RMS)	100 ppm	L = 150 m, D = 129 mm/280 g	≤0.015°/√h	±60°/s	Fizoptika [VG035Q]/ [29]	Platform stabilization
IFOG	High-end tactical	0.1–1°/h	0.10°/h (RMS)	100 ppm	L = 200 m, D = 160 mm/320 g	≤0.007°/√h	±60°/s	Fizoptika [VG951]/ [29]	Missile navigation
RFOG	Low-end tactical	0.1–1°/h	0.10°/h (RMS)	No data	L = 100 m, D = 50.8 mm/no data	≤0.029°/√h	No data	Honeywell [RFOG], [30]	Commercial navigation
IORG	Low-end tactical	1–30°/h	10°/h	< 10,000 ppm	volume < 5 cm³/weight < 100 g/no data	<0.1°/√h	±100°/s	IntelliSense [VIGOR], [8]	Ammunitions and rocket guidance
IORG	Low-end tactical	1–30°/h	1.432°/h	344.71 ppm	60 mm ring resonator Ø/no data/76 μs	0.8°/√h	±300°/s	Feng et al. [31]	Ammunitions and rocket guidance
IFOG	Consumer	30–1000°/h	≤180°/h	≤2000 ppm	No data/no data/50 Hz	≤0.04°/√h	±60°/s	Hitachi Cable [HOFG-1]	Robotics
IFOG	Low-end tactical	1–30°/h	≤1.00°/h	<2000 ppm	60 mm × 60 mm × 19.5 mm (L × W × H)/85 g	<0.1°/√h	±300°/s	Lockheed Martin (NEDAERO) [FOG-60, FOG-80]	AHRS aircraft, ground vehicles, robotics, platform stabilization (antennas)
IFOG	High-end tactical	0.1–1°/h	≤0.05°/h	<50 ppm	90 mm × 90 mm × 88 mm/ 655 g/440 Hz	<0.012°/√h	± 490°/s	Advanced Navigation [SPATIAL FOG]	Surveying applications, robot navigation, ground vehicle positioning
IFOG	Navigation	0.01–0.1°/h	< 0.02°/h (short-term) < 0.20°/h (long-term)	<150 ppm	Ø2.7" × 2″ (11.5 in⁻)/0.8 lb. (362.87 g)/>40 kHz	<0.0022°/√h	± 360°/s	Lockheed Martin (IFOS) [G5-G7-G8-G9 prototypes]	Aeronautics navigation

IFOG/ IORG gyro technology	Performance grade/bias stability range		IFOG/IORG parameters					Manufacturer [model]/ researcher ref. [X]	Applications
			Bias stability	Scale factor linearity	Dimensions/weight/response time	ARW	Dynamic range		
IFOG	Strategic	0.0001–0.01°/h	<0.0003°/h	<100 ppm	No data	$<0.000053°/\sqrt{h}$	From 0.0015°/ h up to 1500°/ h	Lockheed Martin (Optiphase) [prototype's specification]	Submarine navigation, space positioning and navigation
IORG	Low-end tactical	1–30°/h	≤10°/h	< 10,000 ppm	Volume < 5 cm^3/ weight < 100 g/no data	$<0.1°/\sqrt{h}$	± 100°/s	IntelliSense [VIGOR], [8]	Ammunitions and rocket guidance
IORG	Low-end tactical	1–30°/h	1.432°/h	344.71 ppm	60 mm ring resonator Ø/no data/ 76 μs	$0.8°/\sqrt{h}$	± 300°/s	Feng et al. [31]	Ammunitions and rocket guidance
IORG	High-end tactical	0.1–1°/h	0.20°/h	No data	94.8 mm cavity length	$0.00075°/\sqrt{h}$	No data	Ciminelli et al. [24–32]	Aerospace/defense industry

Table 2.
IFOG and IORG gyro technology comparison in terms of performance parameters.

7. Conclusions

IFOGs have higher resolution performance than RFOG and IORG gyros. Therefore, IFOG technology is the best option for strategic-grade (0.0001°/hr), navigation-grade (0.001°/hr), or high-end tactical-grade (0.01°/hr) applications. Best RFOG designs reach high-end tactical-grade (0.01°/hr) or tactical-grade (0.1°/hr) performance, and they constitute a mature and tested technology for a large set of applications ranging from aircraft navigation up to platform stabilization. On the other hand, IORG technology is not yet mature, and over the last decade, it has experienced a vigorous development and refinement. Best results obtained experimentally in the laboratory for the performance of IORG prototypes are of 0.20°/h resolution and $0.00075°/\sqrt{hr}$ARW, respectively. As already mentioned above, several prototypes of RMOGs based on silica resonators have been already theoretically engineered, but the experimentally demonstrated performance is still at least one order of magnitude worse than that one demanded by aerospace and defense navigation applications. Therefore, an improvement of those kinds of gyros is needed to realize a significant impact on the market.

Acknowledgements

Author details

Ramón José Pérez Menéndez
UNED-Spain, Lugo, Spain

*Address all correspondence to: ramonjose.perez@lugo.uned.es

IntechOpen

References

[1] Armenise MN, Passaro VMN, De Leonardis F, Armenise M. Modeling and design of a novel miniaturized integrated optical sensor for gyroscope applications. Journal of Lightwave Technology. 2001;**19**(10):1476-1494

[2] Ciminelli C, Peluso F, Armenise MN. A new integrated optical angular velocity sensor. In: SPIE Conference on "Integrated Optics: Devices, Materials and Technologies IX", San Jose (USA), January. 2005

[3] Suzuki K, Takiguchi K, Hotate K. Monolithically integrated resonator microoptic gyro on silica planar lightwave circuit. Journal of Lightwave Technology. 2000;**18**(1):66-72

[4] Li G, Winick KA, Vikjaer EAJ. Design, fabrication and characterization of an integrated optic passive resonator for optical gyroscopes. In: ION 60th Annual Meeting 2004. June 2004

[5] Ford C, Ramberg R, Johnson K. Cavity element for resonant micro optical gyroscope. IEEE AES Systems Magazine. December 2000;**15**(12):33-36

[6] Armenise MN, Armenise M, Passaro VMN, De Leonardis F. Integrated optical angular velocity sensor. In: Politecnico di Bari, European Patent EP 1219926. 2000

[7] Korkishko Y, Fedorov V, Prilutskiy VE, Ponomarev VG, Morev IV, Obuhovich DV, et al. Investigation and identification of noise sources of high precision fiber optic gyroscopes. In: 20th Saint Petersburg International Conference on Integrated Navigation Systems. 2013

[8] Monovoukas C, Swiecki A, Maseeh F. Integrated optical gyroscopes offering low cost, small size and vibration immunity. In: Proceedings of SPIE 3936, Integrated Optics Devices IV (24 March). 2000

[9] Pavlath G. Fiber optic gyros: The vision realized. In: 18th International Conference on Optical Fiber Sensors, Cancun, Mexico. 2006

[10] KVH Industries Inc. An update on KVH fiber optic gyros and their benefits relative to other gyro technologies. March 2007

[11] Divakaruni S, Sanders S. Fiber optic gyros—A compelling choice for high accuracy applications. In: 18th International Conference on Optical Fiber Sensors, Cancun, Mexico. 2006

[12] Gaiffe T. From R&D brassboards to navigation grade FOG-based INS: The experience of photonetics/IX sea. In: 15th Optical Fiber Sensors Conference Technical Digest. Vol. 1. May 2002. pp. 1-4

[13] Wang W, Wang J. Study of modulation phase drift in an interferometric fiber optic gyroscope. Optical Engineering. 2010;**49**(11): 114401

[14] Emge S, Bennett S, Dyott R, Brunner J, Allen D. Reduced minimum configuration fiber optic gyro for land navigation applications. IEEE Aerospace and Electronic Systems Magazine. April 1997;**12**(4):18-21

[15] Komachia M, Sonobe H, Oho S, Ohbu K, Yuhara T, Hizuka H. Secondary-phase modulation method for open loop fiber optic gyroscopes. Applied Optics. 1996;**35**(9):3719-3725

[16] Lefèvre HC, Marten P, Morrise J, Simonpieti P, Vivenot P, Arditty HJ. High dynamic range fiber gyro with all digital signal processing. In: DePaula RP, Udd E, editors. Fiber Optic and Laser

Sensors VIII, Proceedings - Society of Photo-Optical Instrumentation Engineers, 1367. 1990. pp. 72-80

[17] Pavlath GA. Fiber optic gyro based inertial navigation systems at Northrop Grumman. In: Optical Fiber Sensors Conf. Tech. Dig., OFS 2002, Vol. 1. 2002. p. 9

[18] Sanders SJ, Strandjord LK, Mead D. Fiber optic gyro technology trends—A honeywell perspective. In: Optical Fiber Sensors Conf. Tech. Dig., OFS 2002, Vol. 1. 2002. p. 9

[19] Dyott RB, Bennett SM, Allen D, Brunner J. Development and commercialization of open loop fiber gyros at KVH industries. In: IEEE Optical Fibers Sensors Conference, 15th OFS 2002. 2002. pp. 19-22

[20] Jilmore JP, Freier L, Nolan E, Perlmutter M, Bowser M, Maglieri J. Three-axis nested fiber optic gyroscope. Available at: http://www.fibersense.com [Accessed: 21 April 2019]

[21] Dollon M, Cros G, Sevellec A, Antoine P, Muller G, Willemenot E, et al. A new family of IMU based on IFOG technology. In: Proceedings of the V ESA on Spacecraft—Guidance, Navigation and Control, SP 516, Frascati, Italy, 22–25 October. 2002. pp. 41-45

[22] Ezekiel S, Balsamo SR. Passive ring resonator gyroscope. Applied Physics Letters. 1977;**30**(9):478-480

[23] Meyer RE, Ezekiel S, Stowe DW, Tekippe VJ. Passive fiber-optic ring resonator for rotation sensing. Optics Letters. 1983;**8**(12):644-646

[24] Armenise MN, Ciminelli C, Dell'Olio F, Passaro VMN. Advances in Gyroscope Technologies. Heidelberg: Springer-Verlag; 2010

[25] Ciminelli C, Dell'Olio F, Armenise MN. High-Q spiral resonator for optical gyroscope applications: Numerical and experimental investigation. IEEE Photonics Journal. 2012;**4**:1844-1854

[26] IEEE Standard Specification Format Guide and Test Procedure for Single-Axis Interferometric Fiber Optic Gyros. IEEE Std 952-1997, USA; 1997

[27] Korkishko Y, Fedorov V, Prilutskiy VE, Ponomarev VG, Morev IV, Obuhovich DV, et al. Highest bias stability fiber-optic gyroscope SRS-5000. In: 2017 DGON Inertial Sensors and Systems (ISS), Karlsruhe. 2017. pp. 1-23

[28] Available at: http://www.optolink.ru/en/products/single_axis_fog

[29] Fizoptika. Available online: https://fizoptika.com/ [Accessed: 21 April 2019]

[30] Sanders GA et al. Development of compact resonator fiber optic gyroscopes. In: 2017 IEEE International Symposium on Inertial Sensors and Systems (INERTIAL), Kauai, HI. 2017. pp. 168-170

[31] Li H, Liu L, Lin Z, Wang Q, Wang X, Feng L. Double closed-loop control of integrated optical resonance gyroscope with mean-square exponential stability. Optics Express. 2018;**26**:1145-1160

[32] Ciminelli C, Peluso F, Armenise MN. A new integrated optical angular velocity sensor. Proceedings of SPIE. 2005;**5728**:93-100